Modelling of Metallothermic Reactions – Local Reaction Rates during Aluminothermic γ-TiAl-Nb Production

Jan-Christoph Stoephasius, Bernd Friedrich

Although metallothermic reactions are commonly used to produce ferroalloys such as FeV, FeCr or FeNb, the understanding of the reaction mechanism is insufficient to explain several effects during the reaction. At IME Process Metallurgy and Metal Recycling, department and chair of RWTH Aachen University, metallothermic reactions were conducted in laboratory (10 kg) and pilot scale (180 kg) to examine the propagation of the reaction front. It was found, that there exist two subsequent reaction phases with different reaction rates due to the pressure condition in the bulk phase. Depending on the size, density and ignition behaviour of the reaction material and the amount and viscosity of gaseous reaction products, the first or the second phase predominates.

Keywords:

Metallothermic reduction – Modelling – Yield – Local reaction rate – γ-TiAl – Reaction front – Reaction mechanism

Modellierung metallothermischer Reaktionen – Lokale Reaktionsraten bei der aluminothermischen γ-TiAl-Nb-Produktion

Obwohl metallothermische Reaktionen üblicherweise für die Herstellung von Ferrolegierungen wie FeV, FeCr oder FeNb eingesetzt werden, sind die Reaktionsmechanismen nicht ausreichend bekannt, um verschiedene Effekte zu erklären, die bei der Reaktion ablaufen. Am IME Metallurgische Prozesstechnik und Metallrecycling, Institut und Lehrstuhl der RWTH Aachen, wurden metallothermische Reaktionen im Labor- und Pilotmaßstab (10 kg bzw. 180 kg) durchgeführt, um die Ausbreitung der Reaktionsfront zu untersuchen. Es konnte nachgewiesen werden, dass zwei aufeinander folgende Reaktionsphasen existieren, die aufgrund unterschiedlicher Druckverhältnisse in der Schüttung deutlich verschiedene Reaktionsraten aufweisen. Abhängig von Größe, Dichte und Zündverhalten der Reaktionsmischung und der Menge und Viskosität der gasförmigen Reaktionsprodukte herrscht die erste oder zweite Reaktionsphase vor.

Schlüsselwörter:

Metallothermie – Modellierung – Lokale Reaktionsrate – γ-TiAl – Reaktionsfront – Reaktionsmechanismus

Modélisation de réactions métallothermiques – Les vitesses de réaction locale dans la fabrication aluminothermique de γ-TiAl-Nb

Modelación de reacciones metalotérmicas – Velocidades locales de reacción en la producción aluminotérmica de γ-TiAl-Nb

Paper presented on the occasion of the meeting of the GDMB Experts Committee on Rare Metals, November 17-18, 2004, in Aachen.

Introduction

Metallothermic reactions are commonly used to produce ferroalloys like FeV, FeCr or FeNb [1]. Since four years the process is adapted to titanium-alloys in Aachen [2, 3]. In all cases an unnoble metal like Al, Mg, Ca or Si is used to reduce a high melting metal. Such reactions are extremely fast and self propagating. The typical behaviour of many metallothermic reactions is, that after ignition up to about 2/3 of the total reaction time the process runs extremely smooth, only few smoke and nearly no flames are visible (phase 1). After this time, there is a spontaneous strong increase in the reaction rate (phase 2). The smoke formation and flames become violent. Former explanation of this phenomenon was, that the mixture needs a long time to reach the final process temperature and therewith the maximum reaction rate. But this theory neither can explain the spontaneous increase in reaction rate nor the different "bulk ignition time" for different reactor scales. And as the temperature should increase constantly, the reaction rate should follow. Since the mixture is a very good thermal isolator, the total amount of mixture can not influence the temperature in the middle of the reactor during ignition. Therefore, examinations of the local reaction rates inside the reactor have been conducted to develop a new theory which can explain the above described phenomena and reduces the danger of unexpected reaction rates, due to inadequate reactor geometry and fractional void of the mixture.

2 Fundamentals

Since every aluminothermic reaction produces significant amounts of gas like expanding air from the voids in the mixture, evaporating components (metal, slag or lining) and gaseous reaction products, it is necessary to understand the transport mechanism of these products from the reaction front to the system boundary (outer atmosphere). Considering a section of the reaction front which moves vertically down into the mixture, the gaseous products have two alternatives to leave the system. First they can form a bubble at the bottom of the liquid metal and pass through it and the slag bath which lays above this section of the reaction front. In this case the pressure in the gas bubbles and therefore at the reaction front, must exceed at least the sum of atmospheric and metallostatic pressure of the melt (if the surface tension can be neglected). Assuming ideal cylindrical reaction behaviour (Figure 1), the metallostatic pressure can be calculated from the weight of reacted condensed material and the cross-section of the melt as Equation 1 describes.

$$p_{ms}(t) = g \cdot \frac{m_{cond}(t)}{A(t)} \quad (1)$$

($p_{ms}(t)$: metallostatic pressure [Pa]; g: gravitational constant [9.81 $m \cdot s^{-2}$]; $m_{cond}(t)$: amount of reacted condensed material [kg]; A(t): cross-section of the melt [m^2]; t: time [s])

Beside the straight way through the melt, the gaseous products have the second alternative to flow through the not reacted mixture. The necessary pressure is a function of gas velocity, constitution of the mixture and several material properties. It can be calculated from the Ergun equation, which respects laminar and turbulent aspects as seen in Equation 2 [4, 5].

$$\frac{\Delta p}{h} = 150 \frac{(1-\varepsilon)^2}{\varepsilon^3} \cdot \frac{\mu \cdot u}{(\Phi \cdot d_p)^2} + 1.75 \frac{(1-\varepsilon)}{\varepsilon^2} \cdot \frac{\rho_g \cdot u^2}{\Phi \cdot d_p} \quad (2)$$

($\Delta p \cdot h^{-1}$: specific pressure loss [$Pa \cdot m^{-1}$]; ε: fractional void [1]; d_p: particle diameter [m]; ρ_g: gas density [$kg \cdot m^{-3}$]; μ: gas viscosity [Pa·s]; Φ: form factor [1]; u: gas flow rate [$m \cdot s^{-1}$])

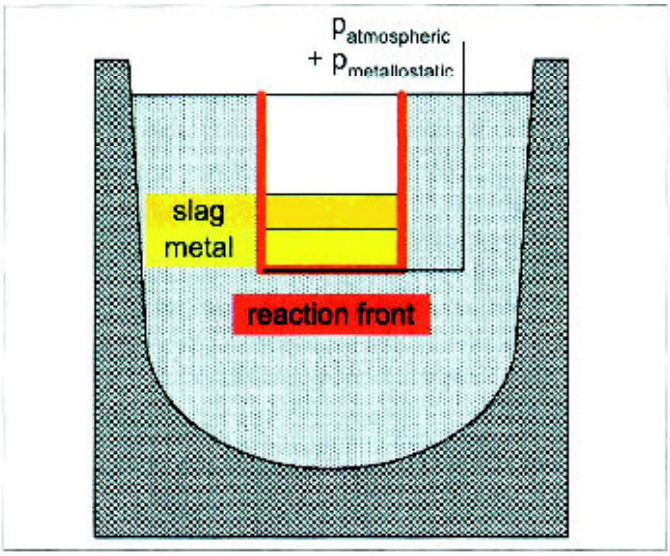

Fig. 1: Aluminothermic reaction with ideal cylindrical reaction behaviour

The fractional void is calculated from the total volume of the input mixture and the volume of the reaction components (here: TiO_2, Al, Nb_2O_5, etc.) using Equation 3. The bulk density of the input mixture was estimated by division of the total mass of input mixture by the used volume in the reactor. It results to 1160 $kg \cdot m^{-3}$, the fractional void ε results to 0.64.

$$\varepsilon = \frac{V - V_{particle}}{V} = \frac{V_{reactor} - y \cdot \pi \cdot r^2 - \sum_i \frac{m_i}{\rho_i}}{V_{reactor} - y \cdot \pi \cdot r^2} \quad (3)$$

(ε: fractional void [1]; V: volume of input mixture [dm^3]; $V_{particle}$: total particle volume [dm^3]; $V_{reactor}$: volume of the reactor [dm^3]; y: distance between the surface of the mixture and the top of the reactor [dm]; r: radius of the reactor [dm]; i: components of the input mixture [Al, TiO_2, …]; m_i: mass of the component i [kg]; ρ_i: density of the pure component i [$kg \cdot dm^{-3}$])

The viscosity of the gaseous products (mainly KCl, assuming that the initial air/humidity is removed by reaction with the liquid Ti-melt) can be calculated from the kinetic theory of gases. [7] Since the total pressure is low and the temperature is high, ideal behaviour can be assumed. The collision diameter σ is calculated from the ionic radii of K^+ (152 pm) and Cl^- (167 pm) and the core distance of KCl (314.6 pm). Above the boiling point of KCl the viscosity can be assumed to be about 95 μPa·s.

$$\mu = 0.499 \cdot m_{particle} \cdot \bar{v} \cdot c \cdot \lambda = 0.998 \cdot \frac{1}{\sigma} \cdot \sqrt{\frac{k \cdot T \cdot m_{particle}}{\mu}} \quad (4)$$

(μ: gas viscosity [Pa·s]; $m_{particle}$: mass of one single gas particle [kg]; $\bar{v}$: medial gas velocity [$m \cdot s^{-1}$]; c: concentration of gas particles [m^{-3}]; λ: medial free length of path [m]; σ: collision diameter [m^2]; k: Boltzmann constant [$1.38 \cdot 10^{-23}$ $J \cdot K^{-1}$]; T: temperature [K])

Due to a wide varying spectrum of particle size (15 … 750 μm) depending on the different components the medial particle diameter and the form factor can only be roughly estimated. The form factor was assumed to be 0.9 and the medial particle diameter 400 μm. Under this conditions the specific pressure loss in the mixture is described by Equation 5.

$$\frac{\Delta p}{h} = 54\,250 \cdot u + 3540 + u^2 \quad (5)$$

($\Delta p \cdot h^{-1}$: spec. pressure loss [$Pa \cdot m^{-1}$]; u: gas flow rate [$m \cdot s^{-1}$])

Figure 2 compares the pressure values needed for different gas velocities, bulk heights and metal/slag layers to pass through the solid phase and through the liquid phase. It can be seen that for low gas speeds ($u < 0.1$ $m \cdot s^{-1}$) the gas pressure in the reaction front is lower than estimated from the metallostatic pressure and therefore the way through the mixture is easier than through the metal bath (Equation 1). For higher gas speeds ($u > 0.15$ $m \cdot s^{-1}$) the metallostatic pressure becomes lower than the pressure necessary for flowing through the mixture, and gas will bubble through the melt.

Once the gaseous products flow through the mixture, it must be considered if their impact on the mixture can lead

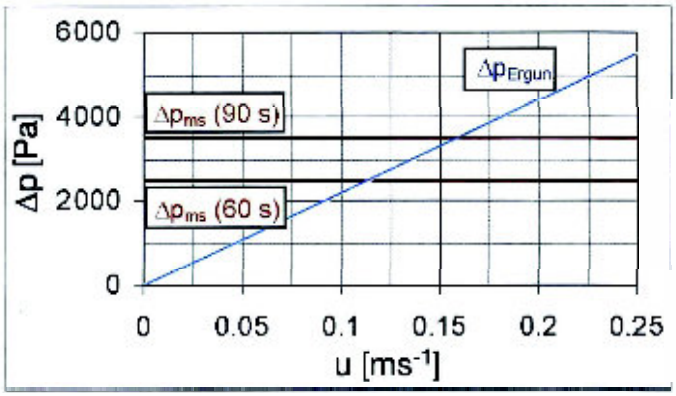

Fig. 2: Metallostatic pressure Δp_{ms} after 60 and 90 s and flowing pressure Δp_{Ergun} as function of the gas velocity ($\varepsilon = 0.64$)

to formation of fluidised beds or even pneumatic transport of single particles. Two equations can be derived from the Ergun equation which allow the calculation of the necessary gas velocity for loosening the particles (Equation 6) and for reaching the pneumatic transport condition (Equation 7) [6].

$$u_{Lo} = \frac{\varepsilon^3}{(1-\varepsilon)} \cdot \frac{g \cdot (\rho_p - \rho_g) \cdot (\Phi \cdot d_p)^2}{150 \cdot \mu} \quad (6)$$

$$u_{pt} = \frac{d_p^2 \cdot g \cdot (\rho_p - \rho_g)}{18 \cdot \mu} \quad (7)$$

(u_{Lo}: loosening velocity [m·s^{-1}]; u_{pt}: pneumatic transport velocity [m·s^{-1}]; ε: fractional void [1]; g: gravitational constant [9.81 m·s^{-2}]; d_p: particle diameter [m]; ρ_p: particle density [kg·m^{-3}]; ρ_g: gas density [kg·m^{-3}]; μ: gas viscosity [Pa·s]; Φ: form factor [1])

Taking the mean particle size into account for all used materials beside aluminium the loosening velocity is below or close to 0.1 m·s^{-1}. This means that the gaseous product flow can loose the input mixture and increase the fractional void. This reduces the flow resistance of the mixture and due to the decreasing pressure loss, the gas speed can increase (Figure 3). At 4.3 mm·s^{-1} the condition of pneumatic transport is reached for the CaO and between 0.9 m·s^{-1} and 1.6 m·s^{-1} all other particles of the input mixture (beside aluminium) can be blown out.

Due to the increasing area of the reaction front, the reaction rate increases and the area of not reacted mixture decreases. It can be assumed, that shortly before the reaction front reaches the lining of the reactor, there is a critical moment in which the gas can not be transported through the mixture anymore due to a too high necessary gas speed. In this moment the pressure rises until the metallostatic pressure is reached and the gas bubbles through the melt. Because of the higher pressure, the reaction rate increases significantly.

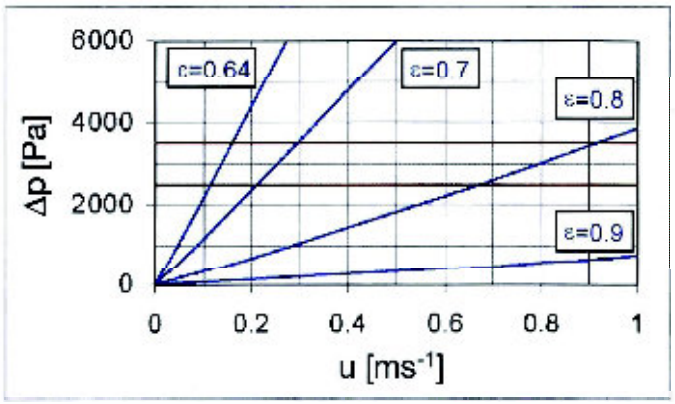

Fig. 3: Metallostatic pressure Δp_{ms} after 60 and 90 s and flowing pressure Δp_{Ergun} as function of the gas velocity and different fractional voids

In phase 1 of the metallothermic reaction while the gas moves through the unreacted mixture, the process stability is low. As Figure 4 shows the gas velocity rises locally by factor 3, if the fractional void of that particular volume of the mixture increases about 0.1. The pressure drop is transferred into gas speed. The impact on the single particle rises by factor 9, as can be seen from Equation 8. This results in a local transcending of the pneumatic transport velocity and formation of funnels. Since the higher mass transfer through the funnel will decrease the gas transport through the surrounding mixture, the surrounding mixture will remain stable, but from the walls of the funnel significant amounts of mixture will be blown out.

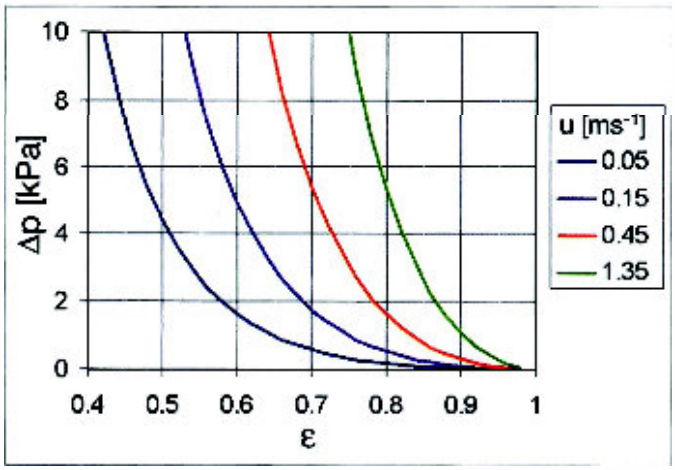

Fig. 4: Dependency of pressure loss from fractional void and gas velocity (Calculation for the IME-reactor, dimensions, see Figure 10)

$$F_w = c_w \cdot A \cdot 0.5\,\rho \cdot u^2 \quad (8)$$

(F_w: flow resistance [N]; c_w: flow resistance coefficient [1]; A: particle cross section [m^2]; ρ: gas density [kg·m^{-3}]; u: gas velocity [m·s^{-1}])

Experimental

3.1 Observation of a small-scale reaction

In a first experiment a small-scale-reaction (10 kg mixture) was conducted in a steel drum which was lined with 100 mm Al_2O_3-based refractory material and finished with ZrO_2. The aim was to retain more information about the reaction behaviour of aluminothermic reactions. A digital video camera was used to record the experiment. By single frame analysis the velocity of smoke and flames was estimated at characteristic times.

The electrical ignition at the top of the mixture leads to a short throwing out of material (Figure 5). The reaction starts very smooth. Only small flames are visible. It can be observed, that on the surface of the not reacted mix-

Fig. 5: Ignition of the mixture (1.4 s)

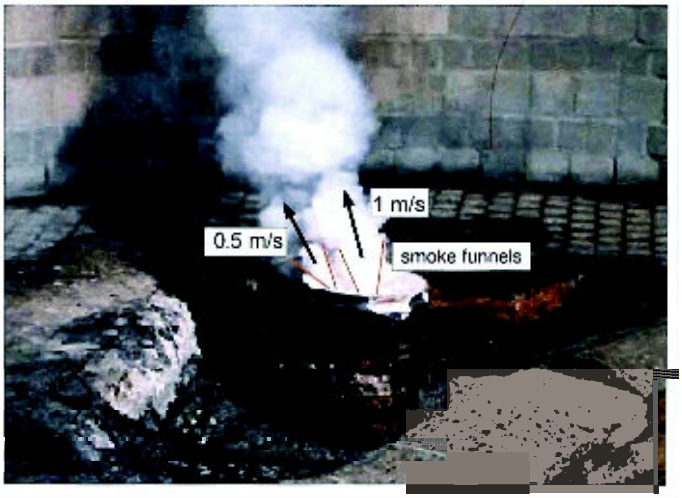

Fig. 6: Smooth reaction, formation of smoke funnels (20.48 s)

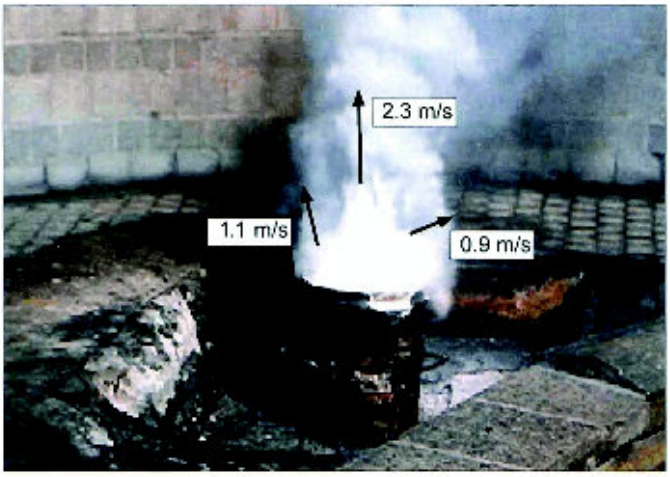

Fig. 7: Critical moment, throw-off of not reacted mixture (56.28 s)

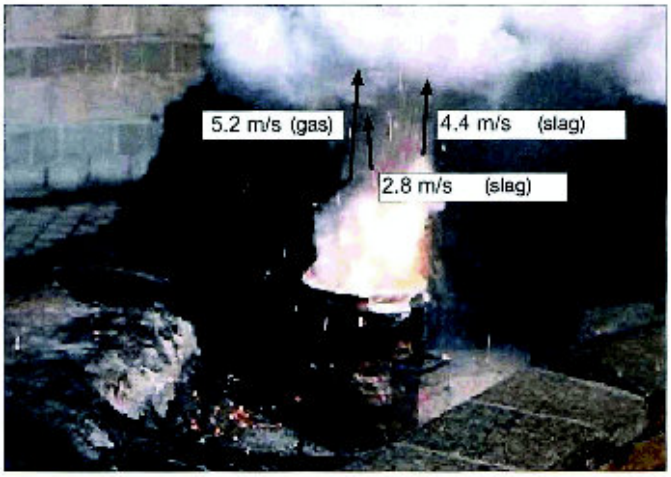

Fig. 8: Full reaction, throw-off of slag (65.56 s)

Fig. 9: Simmered down reactor 1/2 minute after the end of the reaction (102 s)

ture two smoke funnels are formed (Figure 6). The smoke velocity in this funnels was evaluated by the single frame analysis to be 0.5 and 1 $m \cdot s^{-1}$, respectively. After 56 s there is a spontaneous increase in smoke formation and during several short pressure impulses significant amounts of the reaction mixture are thrown out (Figure 7). The smoke velocity increases to 0.9 respectively 2.3 $m \cdot s^{-1}$ at this time. After 65 s the reactivity reaches it's maximum (Figure 8). Instead of not reacted mixture, slag is thrown out with a speed of 2.8 to 4.4 $m \cdot s^{-1}$. The smoke velocity is about 5.2 $m \cdot s^{-1}$. The flames exceed the top of the reactor for more than 0.5 m. Only few seconds later the reaction is completed, the flames disappear and smoke formation decreases strongly. After 100 s the reactor is simmered down and nearly no change can be observed during cooling down for the next minutes (Figure 9).

3.2 Measuring of the local reaction rates

The small scale experiment only gave indirect information about the process. The propagation of the reaction front could not be observed directly. Exact conclusions about the dependency of the reaction rate from influences like the gas pressure were not possible. Therefore, an experimental set up was developed to measure the propagation of the reaction front directly in a pilot scale reactor (ø 650 mm). The total amount of reaction mixture (here to produce γ-TiAl-Nb) was 180 kg.

Four steel-cased backbones were brought into the reactor (cross-section: Figure 10). Each of them contained 14 flat cables which were protected with aluminium sheets against penetrating melt. The backbones were filled with MgO lining material and welded to the reactor to prevent any motion during the process. The flat cables were horizontally

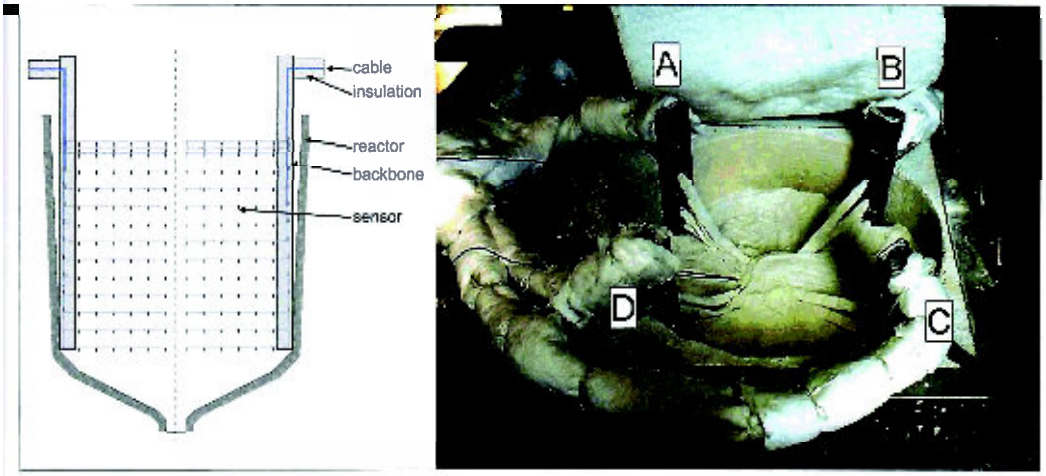

Fig. 10:
Experimental set up for measuring of the local reaction rates (four backbones A-D with each 84 resistor sensors)

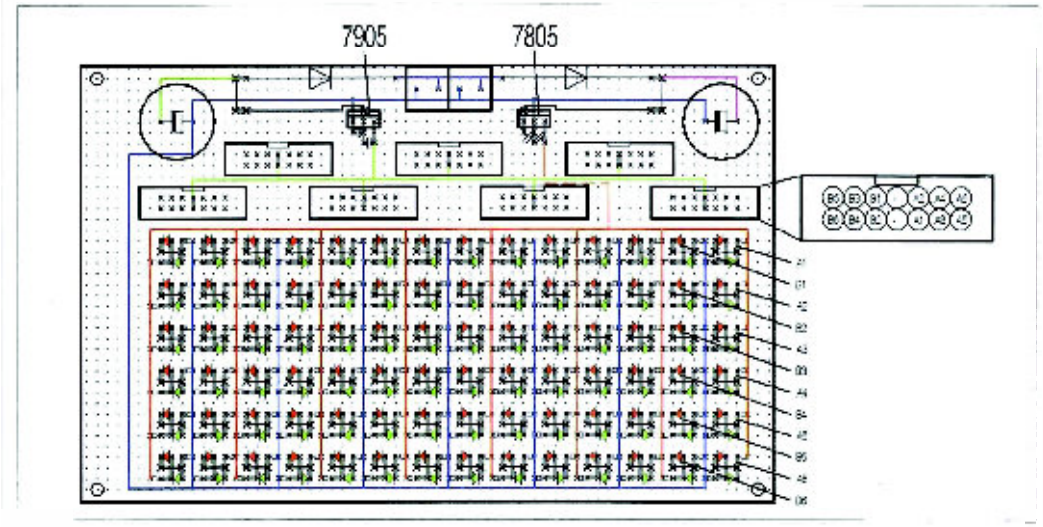

Fig. 11:
Analysis circuit for one backbone

arranged in the reactor and contained six resistor sensors each. The sensor grid was 45 mm in x- and y-direction. The distance between the three flat cables on the top was 10 mm to receive better information about the ignition phase. The flat cables and each sensor were protected individually against the hot reaction gases by several layers of an 1 mm SiO_2-insulation mat.

336 sensors were connected with an analysis circuit (Figure 11) in which for each sensor three different states could be detected and shown with two LEDs (dark = initial state, green = short circuit, red = no contact). From a 6 V AC current supply a stabilized +/- 5 V DC current is generated. A red and green LED are anti-parallelly connected via two resistors with plus voltage. Between these resistors and minus voltage the resistor sensors are connected.

A digital video camera was used to collect the data with 25 frames per second. A second camera was used to observe the reactor. The reaction behaviour was absolutely comparable to the small scale experiment. The protocol is given in Table 1.

For each sensor the time in which the red and the green LED glowed significantly for the first time were recorded. The green LED (short circuit) is the more trustable signal for the reaction front, because liquid slag as well as liquid metal, solid metal and gas plasma from the flame lead to a short circuit. Therefore, only the signals from the green

Tab. 1: Observations from the second camera during pilot-scale experiment

Reaction time [s]	Observation
0	Ignition, white glaring flash from ignition mixture
20	Reaction of ignition mixture finished, reaction becomes smooth, small flame, few smoke
50	No flames are recorded, only smoke visible
68	Small flames appear again, few smoke
76	Several marginal gas evaporation impulses, more smoke
97	Heavier gas evaporation impulses, slag throw-off, much smoke
103	No reactor outline visible anymore due to smoke formation, camera signal becomes dark
124	Very bright camera signal
134	Camera signal becomes dark, end of reaction

LEDs were used to define the location of the reaction front. The local velocity of the reaction front could now be calculated from the time difference and the distance between two neighbouring sensors of the grid. With this information it was possible to interpolate the shape of the reaction front between the points of the grid at fixed times. The result of this interpolation is given for defined times in Figure 12.

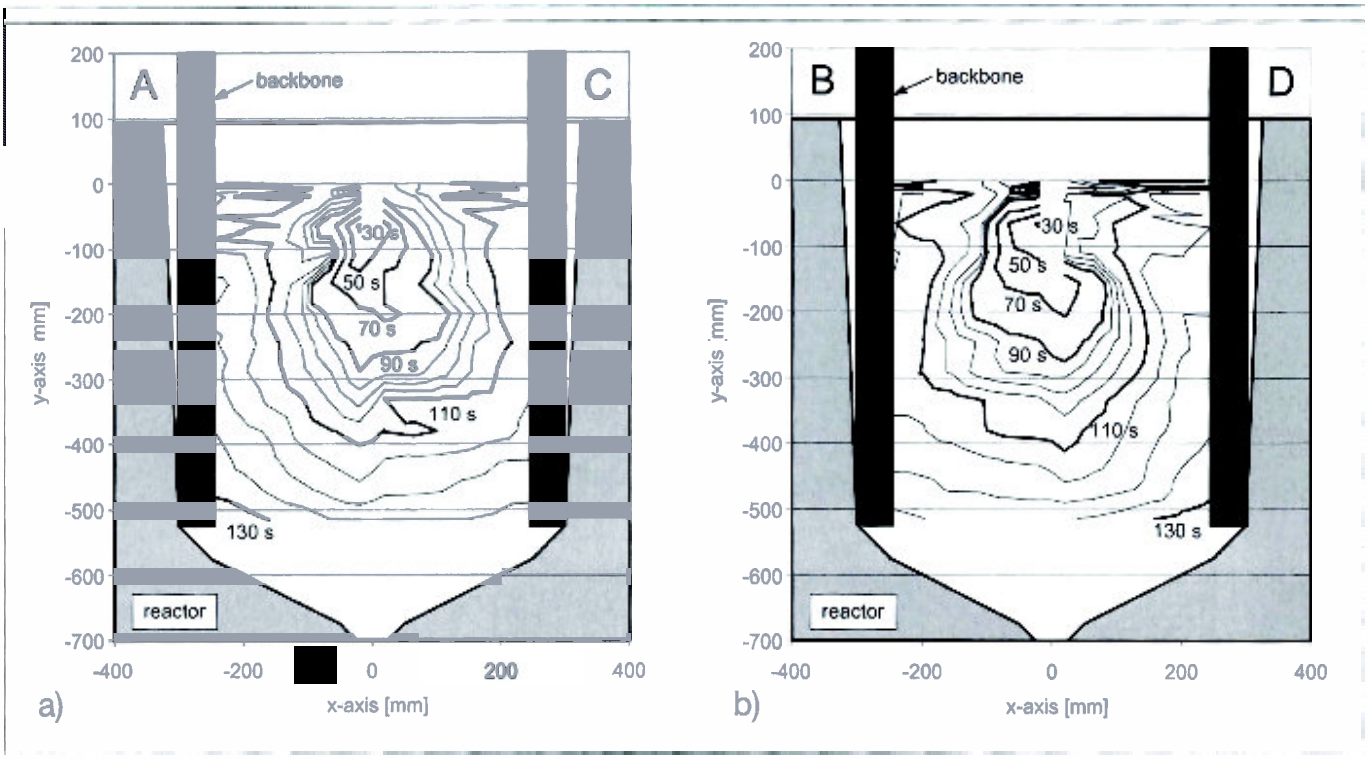

Fig. 12: Cross section between the A-C backbones (a) and the B-D backbones (b) with the interpolated shape of the reaction front based on 336 LED sensors showing short circuit

It can be seen, that it takes 30 s after initial ignition to get the first response from the A and B backbone about 70 mm below the surface of the mixture. This is about 30 mm deeper than the igniting cap was positioned. This shows, that although the ignition reaction is strong exothermic and produces a large flame, there is no deep impact into the reaction mixture. For the next 60 s the reaction front moves slowly downwards. In the bottom part of the reacted area the reaction front moves sidewards with about half of the velocity in y-direction, while in the top part of the reacted area the propagation in x-direction is only very low. 90 to 110 s after ignition the signals become very indifferent (strong oscillation) in the top area of the reactor. The reason for this could be the throw-off of material which impacts the sensor cables. After this period the reaction rate increases significantly. Due to the higher reaction rate and the rising area of the reaction front, the amount of reacted material increases strongly. During the first 80 % of the total process time only 20 .. 25 % of the input material is reacted.

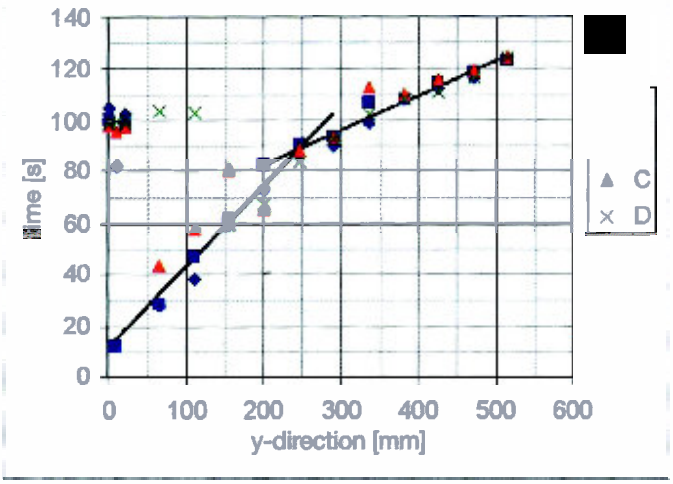

Fig. 13: Progress of the reaction front in y-direction

The progress of the reaction front in y-direction is visualized in Figure 13. The points around 100 s at the top of the reactor are not accounted for the calculation of the local reaction rate, since they belong to the indifferent range mentioned above. The first 250 mm the reaction front moves rather slowly and the velocity shows no significant transition. According to Figure 12 the higher velocity level is reached earlier for the B and C backbone, since the reaction front reaches quicker the reactor lining than at the A and D backbone due to not exactly centered ignition of the reaction mixture.

The local reaction rate in y-direction was calculated from Equations 9 and 10, respectively.

$$u = \frac{d}{\Delta t} \tag{9}$$

(u: local reaction rate [mm·s^{-1}]; d: distance between two sensors [mm]; Δt: time between response of the two sensors [s])

$$r = \frac{d}{\Delta t} \cdot \rho_{mixture} \tag{10}$$

(r: local reaction rate [kg·m^{-2}·s^{-1}]; d: distance between two sensors [m]; Δt: time between response of the two sensors [s]; $\rho_{mixture}$: density of the mixture [kg·m^{-3}])

During the low velocity reaction phase the local reaction rate was 3.19 mm·s^{-1} and 3.7 kg·m^{-2}·s^{-1}, respectively (R^2 = 0.99). During the high velocity reaction phase the local reaction rate was 7.47 mm·s^{-1} and 8.67 kg·m^{-2}·s^{-1}, respectively (R^2 = 0.97).

4 Summary and outlook

Many metallothermic reactions need a period of up to about 2/3 of the total process time to reach the final reaction rate. In this work it was proofed, that this can not be explained with the fact, that the input mixture needs time to reach the final process temperature. The evaluation of the propagation of the reaction front and calculation of the local reaction rate proofed the existence of two independent reaction phases with different reaction rates due to different pressure conditions in the bulk mixture. Depending on the size, density, ignition behaviour of the input material and the amount resp. viscosity of gaseous reaction products the first or the second phase predominates. Due to the large amount of gaseous reaction products but rather slow ignition behaviour, during aluminothermic production of γ-TiAl-Nb alloys both phases can be seen clearly. In the first phase of the total reaction time the gaseous products can move easily through the unreacted mixture and therefore, the pressure in the reaction front is rather low. Since the fractional void is very high, an increasing pressure forces melt to penetrate the unreacted mixture and increase the reaction rate. This happens in the second reaction phase, when there is not enough unreacted mixture left beside the reaction area to allow the produced gases to pass off. Instead they have to overcome the metallostatic pressure of the melt to move through it. Due to decreasing thickness the unreacted mixture beside the reaction front becomes mechanical instable and collapses.

In further experiments a barometer will be used to measure the pressure inside the reaction front online. This equipment allows the evaluation of a direct correlation of reaction rate and pressure. The exact process of the progress of the reaction front from one particle to the next including form factor, size and thermochemical parameters of the particles, pressure, surface tension of the melt, temperature and insteady heat, mass and impulse transfer between the gaseous plasma, the gaseous products and the particles will be modelled and analysed in this long term research project at IME, Aachen. It is the target to introduce a general model for description of the kinetics and prediction of the duration and strength of metallothermic reactions.

Literature

[1] Stoephasius, J.-C. & Friedrich, B. (2004): Modellierung metallothermischer Reaktionen – Berechnung der Einsatzmischung unter Berücksichtigung energetischer Effekte. – ERZMETALL, **57**: 177-184.

[2] Friedrich, B. & Hammerschmidt, J. (2001): Elektroschlackeumschmelzen von aluminothermisch hergestellten Titan-Aluminiumlegierungen – eine Alternative zum Kroll-Prozess? – BHM, **149**: 203-209.

[3] Stoephasius, J.-C., Friedrich, B. & Hammerschmidt, J. (2004): A new Processing Route for Titanium Alloys by Aluminothermic Reduction of Titanium Dioxide and Refining by ESR. – In: Lütjering, G. & Albrecht, J. (eds.): Ti-2003 Science and Technology; Weinheim (Wiley-VCH-Verlag).

[4] Ergun, S. (1952): Fluid flow through packed columns. – Chemical Engineering Progress, **48**: 89-94.

[5] Niven, R.K. (2002): Physical insight into the Ergun and Wen & Yu equations for fluid flow in packed and fluidised beds. – Chemical Engineering Science, **57**: 527-534.

[6] Friedrich, B. (2004): Umdruck zur Vorlesung Metallurgische Prozesstechnik und Metallrecycling; Aachen (IME Metallurgische Prozesstechnik und Metallrecycling, RWTH Aachen).

[7] Neuschütz, D. (1999): Umdruck zur Vorlesung Thermochemie; Aachen (MCh Lehrstuhl für Werkstoffchemie, RWTH Aachen).

[8] Friedrich, B., Hammerschmidt, J. & Stoephasius, J.-C. (2002): Untersuchungen zur Raffination aluminothermisch hergestellter TiAl-Elektroden in einer Elektroschlackeumschmelzanlage; Aachen (Diplomarbeit am IME Metallurgische Prozesstechnik und Metallrecycling, RWTH Aachen).

[9] Hammerschmidt, J. (2003): Entwicklung einer Prozessroute zur Herstellung von γ-TiAl-Legierungen durch Aluminothermie und Schutzgas-Elektroschlackeumschmelzen; Aachen (Dissertation der RWTH Aachen, Shaker Verlag) – ISBN 3-8322-1971-4.

Dipl.-Ing. Jan-Christoph Stoephasius
Prof. Dr.-Ing. Bernd Friedrich
IME Metallurgische Prozesstechnik und Metallrecycling
RWTH Aachen
Intzestraße 3
D-52056 Aachen
JStoephasius@ime-aachen.de